Kinetic Monte Carlo Simulation of Metallic Nanoislands Grown by Physical Vapor Deposition

Abuhanif K. Bhuiyan[1,2], S. K. Dew[1] and M. Stepanova[2,*]

[1] *Department of Electrical and Computer Engineering, University of Alberta, Edmonton, Alberta, Canada T6G 2V4.*
[2] *National Institute for Nanotechnology NRC, Edmonton, Alberta, Canada T6G 2M9.*

Abstract. We report kinetic Monte-Karlo (KMC) simulation of self-assembled synthesis of nanocrystals by physical vapor deposition (PVD), which is one of most flexible, efficient, and clean techniques to fabricate nanopatterns. In particular, self-assembled arrays of nanocrystals can be synthesized by PVD. However size, shape and density of self-assembled nanocrystals are highly sensitive to the process conditions such as duration of deposition, temperature, substrate material, etc. To efficiently synthesize nanocrystalline arrays by PVD, the process control factors should be understood in detail. KMC simulations of film deposition are an important tool for understanding the mechanisms of film deposition. In this paper, we report a KMC modeling that explicitly represents PVD synthesis of self-assembled nanocrystals. We study how varying critical process parameters such as deposition rate, duration, temperature, and substrate type affect the lateral 2D morphologies of self-assembled metallic islands on substrates, and compare our results with experimentally observed surface morphologies generated by PVD. Our simulations align well with experimental results reported in the literature.

1 Introduction

Thin film technology is the underlying basis of a wide range of applications ranging from microelectronics to the emerging field of nanotechnology. In particular, self-assembly of

---

*Corresponding author. *Email addresses:* `abuhanif@ualberta.ca` (A. K. Bhuiyan), `steve.dew@ualberta.ca` (S. K. Dew), `Maria.Stepanova@nrc-cnrc.gc.ca` (M. Stepanova)

nanoscale metallic islands on various crystalline materials, or amorphous substrates such as SiO_2, present a strong interest for nanotechnology applications. However, synthesis of functional crystalline nanostructures require a fine control of the nanocrystalline morphology for which, in turn, the dependence of the morphology on the deposition process conditions should be well understood.

The basic physical mechanisms behind the nucleation and growth of deposited films have been extensively addressed in the literature. At the early stages of deposition, incident atoms randomly impinge on the substrate at a given rate, and then the adsorbed atoms can re-evaporate, aggregate, or diffuse [1]. Coalescense of adatoms results in nucleation of tiny nanoislands on the substrate. Islands containing more adatoms than a critical nucleation number [2, 3] give rise to relatively stable nanocrystals, whose size increases due to the arrival of new adatoms at the surface [4]. The evolution of growing islands can be described by kinetic rate equations [4, 5]. For relatively early stages of deposition, some of the rate equations can be solved analytically. The corresponding solutions, known as scaling laws, relate the number density of stable nuclei with the various process and material parameters, as it has been addressed in detail by Venables and coworkers [4–7]. For example, the density of stable islands N in a hypothetical steady state regime is given by,

$$N = An_0 \left(\frac{R}{v} \right)^p \exp \left(\frac{U}{kT} \right),$$ (1.1)

where A is a dimensionless constant, n_0 is the density of adsorption sites at the surface, R is the deposition rate in ML/sec, v is the fundamental frequency, T is temperature, U is the activation energy, and the power p is a parameter depending on the critical nucleation size i. The asymptotic dependence of p on i is usually described by $p = i/(i+2)$ [7, 8].

The scaling laws have proven to describe well the density of stable nuclei at early stages of deposition. Of major interest for applications, however, are detailed morphologies that develop at later stages of the process, when the nuclei grow into nanocrystalline islands. Thus, the experimental morphologies shown in Figs. 1 and 2 demonstrate that the shape of deposited metallic islands depends of the substrate. As it can be seen in Fig. 1, under typical conditions, metal islands deposited by PVD techniques on amorphous substrates such as SiO_2 undertake smooth droplet-like shapes [9]. At later stage of deposition, some of these patterns resemble percolation networks (see the last picture of Fig. 1(a)). In contrast, when a metal is deposited on a crystalline substrate [10–12], the islands adopt more regular "crystal-like" shapes, as shown in Fig. 2. The crystalline morphology persists when temperature increases, which is evident form the images in the figure. It is clear that such differences cannot be captured by the density and/or the average size of islands provided by the scaling laws, and require a more detailed consideration. With continuing deposition, the islands start merging and the pattern evolves into a continuous thin film. These late stages of nanocrystalline synthesis also require appropriate simulation approaches capable to account for the changing surface morphology.
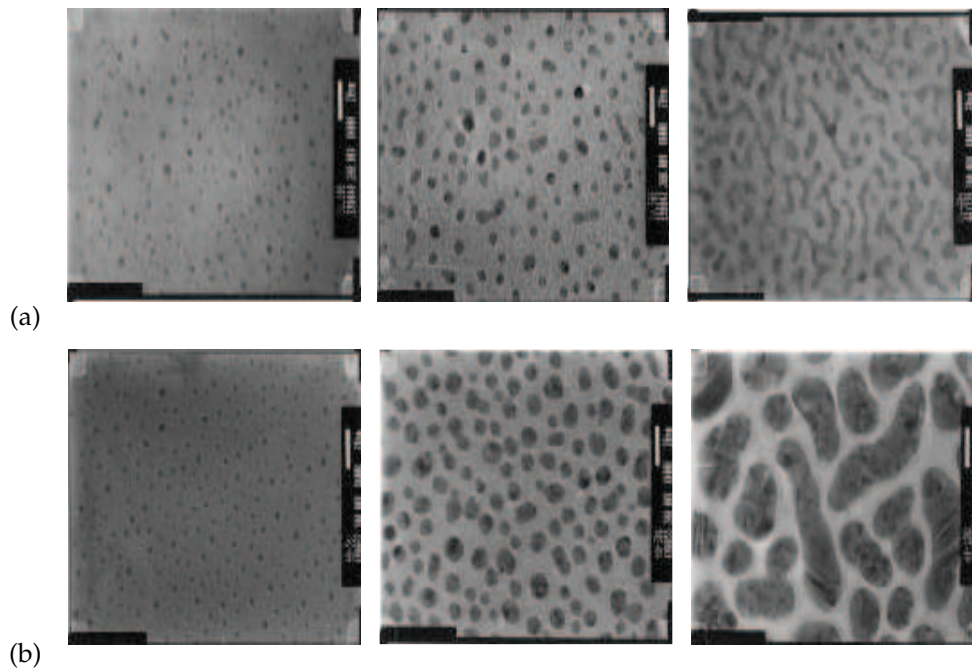
Figure 1: TEM images (200 nm × 200 nm) of nanopatterns on glass (SiO$_2$) at ambient temperature for (a) Cu deposition times of 10, 30 and 60 seconds, and (b) Ag deposition times of 5, 30 and 120 seconds from [9]. (Reprinted with permission of Springer Science & Business Media.)

Detailed understanding and prediction of the effects of the various deposition conditions on the morphology of the growing nanoparticles is important, since the mechanical and electrical properties of nanostructures strongly depend on the sizes and shapes of crystallites involved. For example, the larger the grains are the higher the resistance to electromigration and therefore the longer the life of interconnection [13]. A capacity to control these structural properties by varying the standard process conditions such as the deposition rate or temperature, would result in efficient nanofabrication techniques. Such a control is enabled by insight from comprehensive and systematic theoretical tools. In particular, detailed numerical modeling of self-assembled synthesis of nanocrystals is a subject of constantly growing interest. Popular approaches to such simulation include Molecular Dynamics (MD) simulation [14–16], Kinetic Monte Carlo (KMC) simulation [7,13,17–24], and analytic coarse-grained theories. [25,26]. The performance of these simulation techniques depends on the size, time scale, and details of the process to be studied. KMC favorably combines flexibility, predictive power, and numerical efficiency, and as such is very well suited for both basic understanding of nanocrystal growth and applications for in-silico aided design of nanofabrication processes. For this reason, KMC simulations have been widely used to study nanocrystalline growth. KMC models can be categorized into several groups, including specific event KMC [17,18], bond counting KMC [7,13,19–23], and complete table KMC [24]. Out of these, the bond counting method
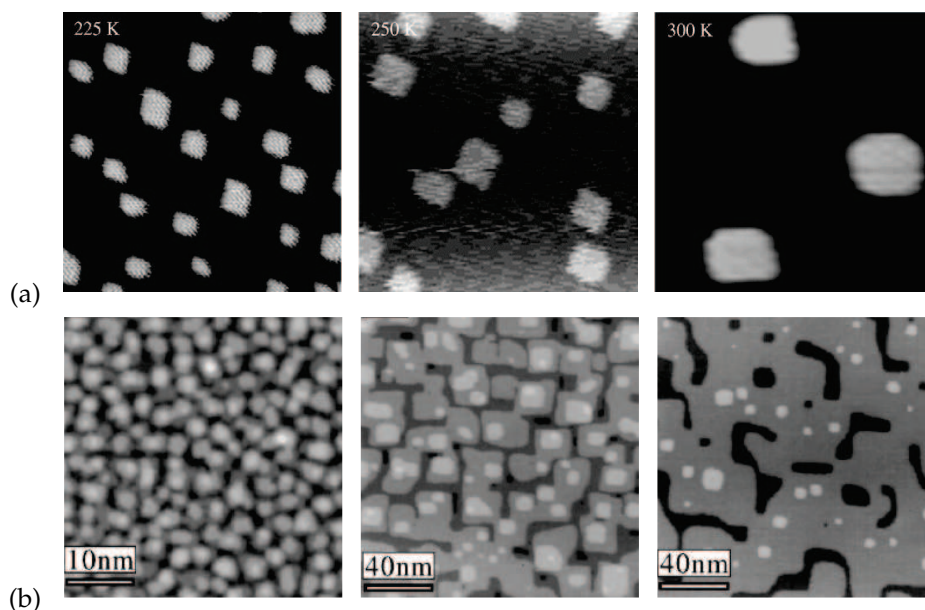
Figure 2: (a) STM images (25 nm × 25 nm) of $\theta = 0.1$ Ag/Ag(100) deposited at 0.006 ML/s at temperatures of 225, 250 and 300 K from [10]. (b) STM image of Fe growing on Fe (100) at temperatures of 293, 453 and 523 K from [12]. (Reprinted with permission of American Physical Society.)

is perhaps the most widely used in relation to film deposition modeling. Advantages of this approach involve a reliable assessment of the ground state of the adatoms, as well as an explicit accounting for the change in the total bond energy when the number of neighbors changes [18].

Most published works reporting KMC modeling, however, address the nucleation regimes that are also accessible to treatment by analytic nucleation theories [7, 13, 17, 20, 21, 23]. A few papers compare KMC modeling directly with similar experimental results [18, 19]. KMC studies pursuing a focused goal of describing the effect of major process control parameters of PVD-based self-assembling synthesis of nanocrystals are less frequent. Accordingly, understanding the impact of the synergy of the deposition conditions on the growing morphology is still incomplete. With the advancement of nanotechnology there is a demand to guide process engineers for a more detailed description of the self-assembling nanostructures, especially grain size, grain shape, grain orientation, and texture.

The motivation for our work is to develop a model capable of representing the specific PVD process aspects for a given set of conditions, and to study the impact of these conditions on the morphology of the deposited nanoislands. In this paper, we focus on a 2D simulation of the nano scale morphologies, using the bond counting KMC method, and targeting PVD processes such as sputtering, evaporation, epitaxy etc. In Section 2 we outline our model; in Section 3 we present and discuss our results, and Section 4 summarizes the outcomes of the work.
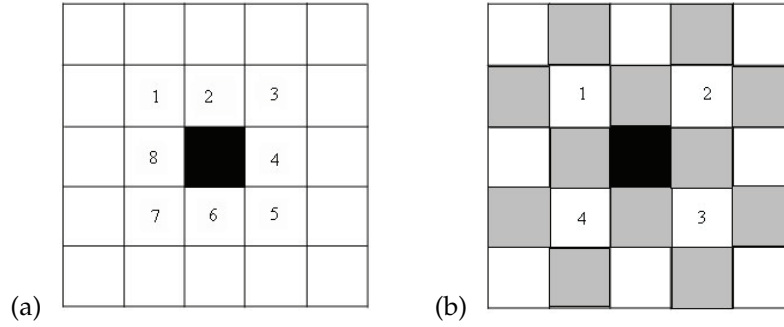
Figure 3: Two models for the lateral interaction of adatoms: (a) Model 1, primitive square lattice and (b) Model 2, FCC lattice. The black rectangles indicate adatom and the numbers indicate the allowed positions for jumping.

2 Model

We model the film deposition-diffusion process for Cu and Ag using two simple square lattice models describing the lateral interaction between adatoms. Model 1 with eight neighboring sites for each atom is simply the primitive square lattice and Model 2 with four neighbors in an alternating formation represents the (100) FCC lattice. The symmetry of the growing metal clusters depends on the type of lattice structure used in the model [27]. Fig. 3 shows the structure for both models. Simulations were performed for an area L × L = 400×400 cells for Model 1 and 566 × 566 cells for Model 2. Periodic boundary conditions were applied. We assume the diameter of an atom equal to 0.25nm [28] to make the simulated region 100 nm on a side. In this work, we only consider 2D morphologies of the growing nanostructures.

We account for the deposition and diffusion processes, which are described by the numbers of corresponding Monte-Carlo steps N_{dep} and N_{diff}. Sites for both deposition and diffusion Monte-Carlo steps are selected at random locations in the 2D array, in such a way that individual deposition and diffusion events are not correlated. For a given period of time t, the number of attempted Monte-Carlo deposition and diffusion steps is determined by

$$N_{dep} = tR, \tag{2.1}$$

and

$$N_{diff} = tD_{adatom}/d^2, \tag{2.2}$$

respectively, where R is the deposition rate in monolayers (ML) per second, and D_{adatom} is the surface diffusivity of adatoms. The adatom diffusivity can be represented by

$$D_{adatom} = D_0 \exp\left(-\frac{E}{kT}\right). \tag{2.3}$$

Here D_0 is the pre-exponential factor, T is temperature, and E is the activation energy

of adatom diffusion in the absence of lateral bonding with other adatoms. The latter is considered to be equal to 0.46 eV for Cu and 0.38 eV for Ag [3, 11].

At each Monte-Carlo deposition step, a randomly selected cell in the 2D array is selected. In the present 2D simulation, the deposition of an atom occurs at the condition that the selected cell is empty. At each Monte-Carlo diffusion step, two nearest-neighbor cells "a" and "b" are also selected randomly considering 8 nearest-neighbors for Model 1 and 4 neighbors for Model 2. Next, we compute the probability $P_{a\text{-}b}$ of jump from position "a" to position "b" through the Metropolis algorithm with the energy function F depending on the number of lateral bonds n in positions "a" and "b" in such a way that $F = yn$, for $n > n_c$ and $F = 0$ for $n < n_c$, where n_c represents the number of bonds for a critical nuclei adopted to be 3 for Model 1 and 2 for Model 2. The corresponding probability of an adatom's jump from position "a" to position "b" is

$$P_{a-b} = \min\left(1, \exp\left(-\frac{y(n_b - 1 - n_a)}{kT}\right)\right), \tag{2.4}$$

where y is the energy of lateral bonds between adatoms, $n_{a,b}$ are the numbers of lateral bonds at neighbor locations "a" and "b", respectively, The energy of lateral bonds between adatoms, y, was derived from the cohesive energies for Cu (3.52 eV) and for Ag (2.95 eV) [29]. Accordingly, for Cu in Model 1, each bond contributes approximately 0.20 eV, and in Model 2 each bond contributes 0.39 eV to the total lateral binding energy. For Ag, the corresponding values are 0.17 eV and 0.32 eV for Model 1 and Model 2, respectively [30]. Cohesive energy provides a reasonable approximation and is often used for calculating the bond breaking energy [31–33]. Because the bond energy y, which describes attractive interatomic bonds, is a negative value, the probability P given by Eq. (2.4) is equal to 1 for jumps resulting in an increasing number of bonds, and is less than 1 otherwise.

The entire process of simultaneous deposition-diffusion is repeated for a number of time cycles, each describing a brief time interval, typically one second. Time in the simulation is scaled according to the number of deposition steps as well as the deposition rate that has been assigned to the system. For a given deposition rate, the number of attempted deposition steps N_{dep} is determined by the deposition time (see Eq. (2.1)), whereas the number of attempted diffusion steps N_{diff} depends on both time and temperature according to Eqs. (2.2) and (2.3). The number of executed diffusion steps includes a further temperature dependence as described by Eq. (2.4). This framework allows us to study the impact of the deposition rate, time, and temperature, as independent factors, on the plan-view surface morphology. For convenience, we also employ a kinetic parameter K, which characterizes the relative influence of the number of attempted deposition and diffusion steps on simulation of the growth process. The value of K is given by the ratio of deposition and diffusion steps in the simulation,

$$K = \frac{N_{dep}}{N_{diff}}. \tag{2.5}$$

This definition is comparable to the so-called lumped parameter employed in the analytic scaling laws [7, 8, 24], which facilitates interpretation of some of the results of the simulation and comparisons with the analytical theory.

3   Results and discussion

Below we present results of our KMC simulation of the PVD deposition of metal clusters on the two model symmetries of the lateral interactions, and study the resulting nucleation and coarsening behavior. The variables include deposition rate, duration, and temperature. Outcomes of the simulation include the average size of metal islands and their 2D shape in the plane of the substrate. We define the size of the islands by their average diameter, calculated as four times the total area of islands divided by their total perimeter. It is a valid approach as long as applied to regimes where the islands adopt nearly circular or nearly rectangular shapes. As it follows from published experiments and is also confirmed by our modeling below, most self-assembled islands have such regular shapes in the broad range of surface coverages, so that our evaluation of the islands size is fairly reliable. We have also analyzed the densities of nanoislands generated. Our results are described below.

3.1   Time evolution of the surface morphology for model substrates

Fig. 4(a) shows the percentage of surface coverage by adatoms and islands, which was determined by dividing the total number of deposited atoms by the total number of sites available in the system, as a function of deposition time for Ag. Obviously, the surface coverage increases with the time of deposition. In Fig. 4(b), the average size of Ag clusters is shown as a function of deposition time for two models for the lateral interactions, and Fig. 5 demonstrates the corresponding evolution of the morphologies. In both models, the size of clusters increases with time. At the room temperature regimes considered in
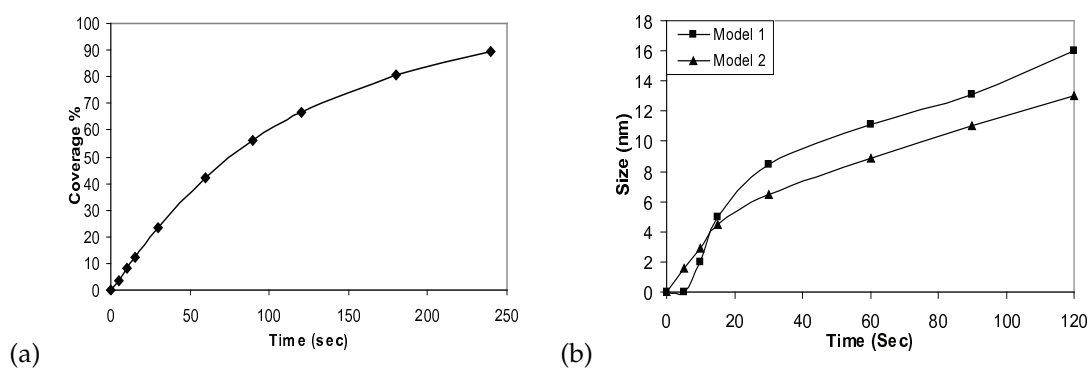
Figure 4: Percentage of substrate coverage (a) and island size (b) as functions of time. Simulations correspond to Ag deposition at $T = 300$ K and $R = 0.0093$ ML/sec.

(a)

(b)

$\theta = 0.05$ $\theta = 0.25$ $\theta = 0.49$ $\theta = 0.68$
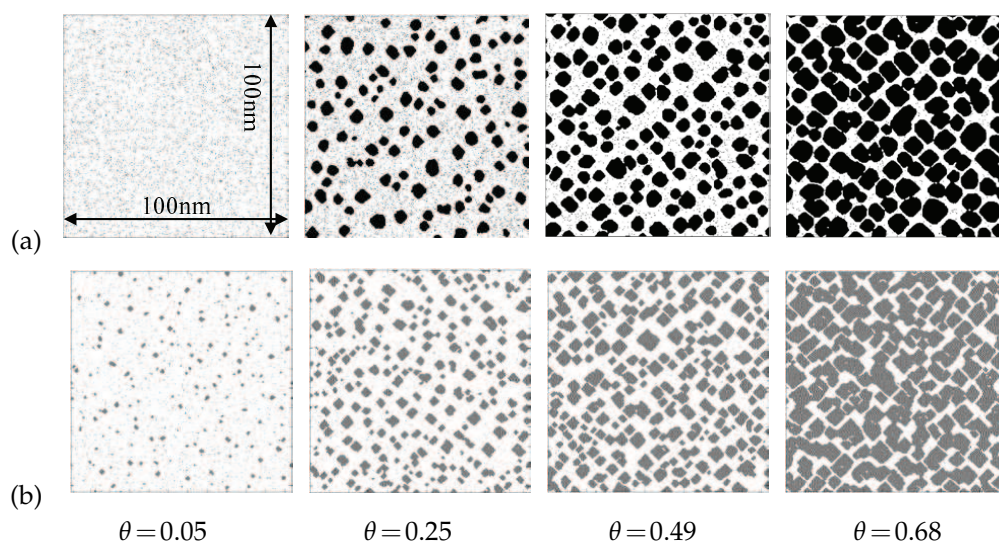
Figure 5: Simulated surface morphologies demonstrating Ag islands' growth for deposition times of 5 sec, 30 sec, 1 minute and 2 minutes for (a) Model 1 and (b) Model 2 at $T = 300$ K, $R = 0.0093$ ML/sec and the surface coverage are shown as "θ" below the figures. The size of the modeled area is 100nm$\times$100nm.

this example, growth occurs mainly because of arrival of deposited atoms at the surface, as well as by coalescence (merging of clusters). Another mechanism that may contribute to cluster's growth, primarily at increased temperatures, is the Ostwald ripening (growth of larger clusters at the expense of smaller ones). Gradually, the growing islands coalesce into a continuous thin film. According to our results, this occurs in about 4 minutes of deposition when the coverage reaches approximately 90%.

As it can be seen in Fig. 4(b), the islands increase in size quickly over the initial period of deposition (approximately 20-30 sec.), after which the growth slows down. The crossover occurs when the average inter-island distance becomes less that the effective diffusion length of adatoms, i.e. the condition at which neighbor islands start competing for capturing newly deposited adatoms. The regimes of slower growth corresponds the best to the conditions of applicability of the analytical scaling law (1) and its derivatives.

The comparison of two models of the lateral interaction in Fig. 4(b) and Fig. 5 shows that nano-islands corresponding to these models largely show a similar behavior. A difference seen in these figures is that with Model 2, islands nucleate at an earlier stage of deposition compared to Model 1. This can be explained by the higher activation energy for adatom diffusion in Model 2. Another notable point is the difference in shapes of clusters with two models, which is clearly seen in Fig. 5. Thus Model 2, which corresponds to FCC symmetry, leads to rectangular islands as expected for crystalline substrates, whereas Model1 produces softer morphologies with rounded corners, reminiscent of deposition onto non-crystalline materials such as glass. Remarkably, the experimentally observed clusters grown on crystalline substrates and glass (see Figs. 1 and 2) show similar morphologic trends as we have obtained. This similarity of the simulated and experimental

morphologies is observed both at early sub-monolayer stages of deposition and for developed coverage, when the deposited structures may contain more than one monolayer of atoms. This confirms that our 2D model is representative of both the submonolayer regimes of deposition as well of its later stages.

From Fig. 5 it is evident that for both substrate geometries, the islands' facets adopt a preferential "diagonal" orientation with respect to the main crystallographic orientations at the surface. In order to understand the origin of this texture, we have considered relevant locations of adatoms either at a corner or at a side of an island for both substrate symmetries, as illustrated by Fig. 6. We identify six typical adatom locations, which are marked by "x" Fig. 6. For each typical adatom location, we determine the number of bonds with its neighbors, m, and compare it with the critical nucleation bond number n_c. If the number of neighbors m is equal or more than the n_c, the atom considered stable in that location.

In Model 1 and case 1, the adatom located at the corner of a straight island is 3 bonded to 3 neighbors. In case 2 the atom located at the side of a straight island has 5 bonds. In case 3, the terrace adatom near the straight island has 3 bonds. In cases 4, 5, and 6, the atoms located in the corner, at the side, and near a terrace of a diagonal island have 3, 5, and 1 bond, respectively. The number of bonds available defines the stability of the atom in that location. For Model 1, the critical bond number (n_c) is equal to 3 (See Section 2). Thus, an atom that has 3 or less neighbors is considered to be in unstable position. In cases 1 & 4, the corner atom has 3 bonds and is also unstable. However in cases 2 & 5, the side atom has 5 neighbors and is bonded firmly with the island. Comparing the side and corner adatom positions in both straight and diagonal islands, it appears that they are equivalent in terms of stability. However a different behavior is observed in the cases of terrace adatoms. In case 3, the straight island terrace adatom has 3 bonds. In such a position adatom is marginally unstable, but addition of only one more adatom would stabilize it. For case 6 diagonal island terrace adatom has only 1 bond, which is an unstable position. As a result, the diagonal terrace is less likely to undergo distortions by attachment of adatoms than the straight terrace. Because of this we observe a preferential diagonal orientation of the islands which, however, show "rounded" corners formed by small segments of straight terraces. Similarly one can analyze the typical positions of adatoms in Model 2. From Fig. 6 it is evident that in distinction to Model 1, only locations at diagonal sides are stable, which naturally results to an even stronger preference of the diagonal texture than in Model 1.

One can conclude that Model 1 allows for a growth in both straight and diagonal directions of the island's boundaries, but the diagonal orientations are more immune to distortions than the straight ones, whereas in Model 2 only the diagonal direction is stable. Thus, the diagonal orientation is the preferred one in both models, as it can be seen in Fig. 5. However, since Model 1 allows the alignments in both directions, the corners of the growing islands are softer and round shaped. In contrast, Model 2 allows for the diagonal direction only, which explains why the corresponding islands seen in Fig. 5 are more uniformly shaped and corners of the islands are sharper than for Model 1.

	Case1: Straight Corner	Case2: Straight Side	Case3: Straight Terrace Adatom
Model 1	$m_1=3$	$m_2=5\ (>n_c)$	$m_3=3$
Model 2	$m_1=1$	$m_2=2$	$m_3=2$
	Case4: Diagonal Corner	Case5: Diagonal Side	Case6: Diagonal Terrace Adatom
Model 1	$m_4=3$	$m_5=5(>n_c)$	$m_6=1$
Model 2	$m_4=2$	$m_5=3(>n_c)$	$m_6=1$
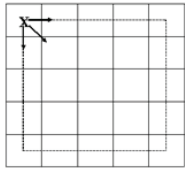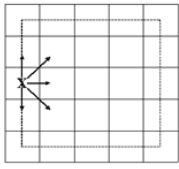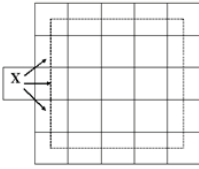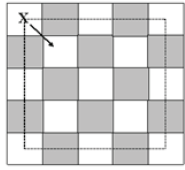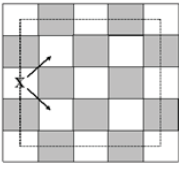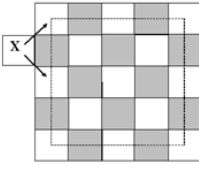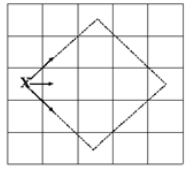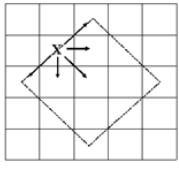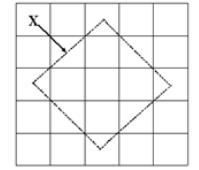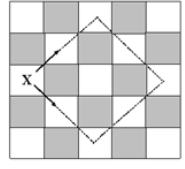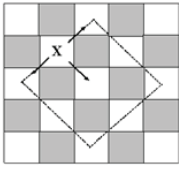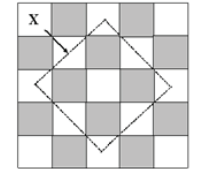
Figure 6: Geometries and numbers of neighbor atoms for 6 characteristic adatom locations in Model 1 and Model 2. Solid arrows show the bonds. Dashed lines indicate boundaries of hypothetical islands.

3.2　Effect of deposition rate

We have studied the effect of the deposition rate R under two representative conditions, constant deposition time and constant surface coverage. First, we simulate deposition during 1 min. with varying deposition rate (i.e. constant deposition time, see Figs. 7(a,b) and 8(a)). As it follows from the figures, below the deposition rate of approximately 0.004 ML/s, the island sizes are very small (Fig. 7(a)) and few in number (Fig. 7(b)), however,
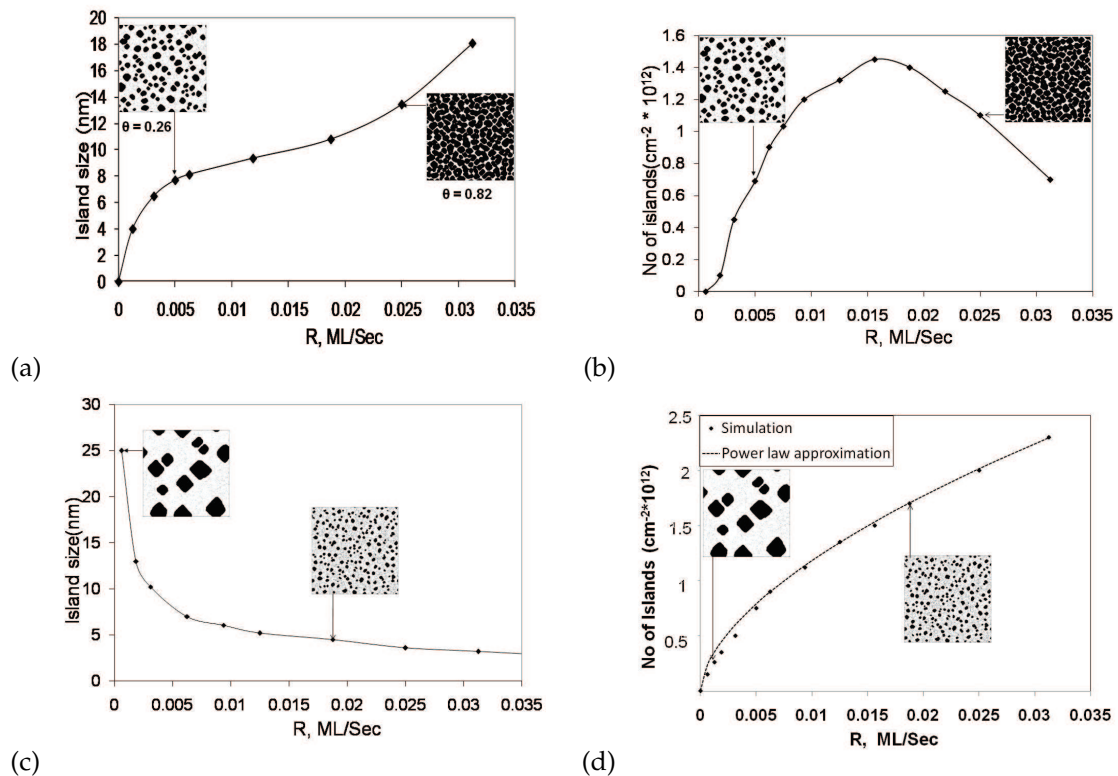
Figure 7: The average size (a,c) and density (b,d) of islands as functions of the deposition rate, for constant 1 min duration of deposition (a,b) and constant 23% coverage (c,d), for Ag deposition using Model 1 at $T = 300$ K. The size of the modeled area shown in the insets is 100nm×100nm.

both the island size and density increase steeply with R. When the rate increases beyond 0.005 ML/s, further change in size is minor, but the density of islands keeps increasing. However, when the deposition rate increases above 0.02, the increase in island size with R is again considerable, whereas and the density decreases sharply. The explanation is that at low deposition rate, the surface density of adatoms is also low. Formation of stable nuclei is a relatively rare event in these regimes, islands are sparse, and most of newly arrived adatoms are available for contributing to the growth of existing islands. The size of islands is limited mostly by the availability of newly arrived adatoms, and increases in proportion to their supply. The plateau regime seen in Fig. 7(a) occurs at the conditions where newly formed stable islands start competing for adatoms with the existing ones. In this regime, the increasing density of islands (see Fig. 7(b)) becomes the limiting factor for their size, which stabilizes as Fig. 7(a) shows. This behavior is also illustrated by the morphologies shown in Fig. 8(a). At high deposition rates, when the surface coverage exceeds approximately 60%, the neighbor islands merge and a continuous thin film starts forming, as it can be seen in Fig. 8(a). This results to a decrease in the nominal island density (Fig. 7(b)) and a pronounced increase in size (Fig. 7(a)). Note however, that the
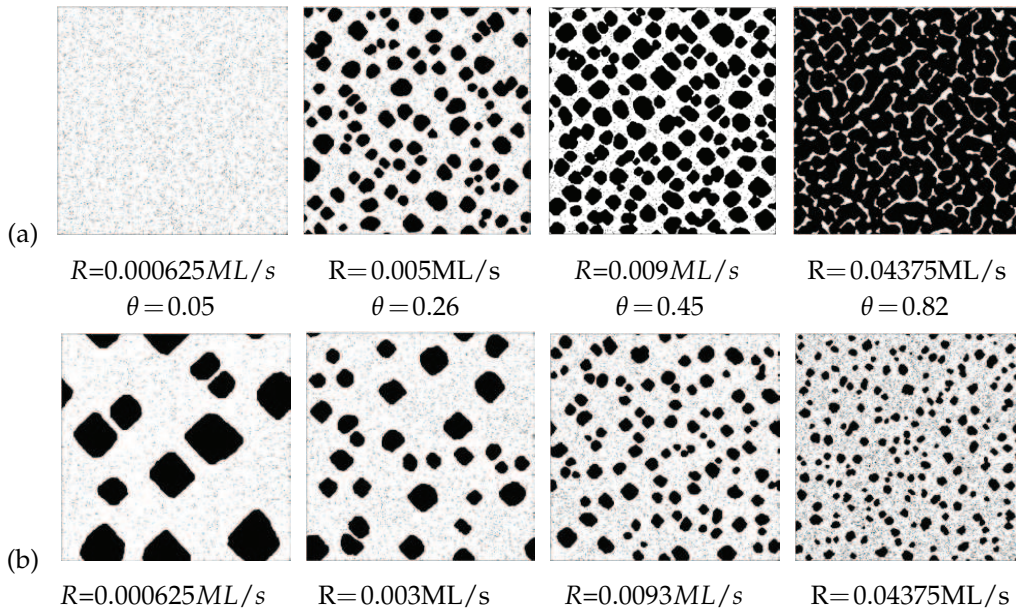
Figure 8: Simulated surface morphologies for Ag deposited during $T=300K$ with varying deposition rates at constant duration of 1 min (a) and constant coverage of 23% (b). The surface coverage for (a) is shown as "θ" below the figures. The size of the modeled area is 100nm×100nm.

accuracy of the approach that we employed to evaluate the island size is limited in this regimes, and thus the increasing portion of the dependence in Fig. 7(a) for high deposition rates R is rather qualitative. However, the overall trends shown by Figs. 7(a,b) and Fig. 8(a) are representative and in lines with the experiments on deposition of Ag on Ag (100) (see, e.g., Fig. 2 and also [9]).

We have also studied the effect of deposition rate while keeping constant the percentage of final surface coverage (see Figs. 7(c,d) and Fig. 8(b)). We observe that at very low deposition rate, only few large islands are formed. As we increase the deposition rate keeping the coverage fixed at the level of 23%, the island size decreases. Initially this change is dramatic, but later its effect is not as significant (Fig. 7(c)). In contrast, the density of islands increases steadily with increasing R as demonstrated in Fig. 7(d) and Fig. 8(b). The last trend results from facilitated nucleation at higher deposition rates, which provides a larger number of stable nuclei per unit area. What concerns the decreasing dependence seen in Fig. 7(c), it may be explained by shorter deposition times required to deposit a particular surface coverage with increasing deposition rate. In this case, the island size is limited by the number of captured adatoms over the time required to reach a 23% surface coverage, which decreases with R.

Analysis of the dependence $N(R)$ shown in Fig. 7(d) shows that it is reasonably well described by the scaling law $N \sim R^{-0.583}$. Although the power of 0.583 is somewhat less than the asymptotic estimate 0.67 that corresponds to the critical number of bonds adopted in our model, one can conclude that the density of islands can be described by

the scaling law (1.1) at the assumption that the surface coverage is kept constant at a relatively low value of 23%. However, the scaling law expressed by Eq. (1.1) is inapplicable to Fig. 7(b), which presents the dependence $N(R)$ at a constant time of deposition.

The conclusion is that variation of deposition rate is a powerful control factor, by which process engineer can direct the process of nanoparticle growth. This process, however, depends over a number of other conditions, such as the time and coverage of the surface, whose impact should be accounted for properly. The well-known classic scaling laws, although very useful for understanding of basic physical trends, are not always flexible enough to capture efficiently all the diversity of deposition. This emphasizes the importance of efficient direct simulations of the deposition process. In addition to more flexibility when describing the average characteristics such as the number of stable nuclei, KMC simulations also provide important information on the detailed morphology of the surface such as shown in Figs. 5 and 8, which is an important component required for a detailed understanding of the trends of deposition, as well as for efficient in-silico aided PVD process design.

3.3   Effect of the kinetic factor *K*

As the next step, we study the impact of the kinetic factor *K* (see Eq. (2.5)) on the results of our simulations. It should be noted that *K* represents the numerical procedure rather that any PVD process control parameters, however, similar descriptors have been employed frequently as a convenient variable in scaling laws [7, 8, 24].

The graph in Fig. 9 shows the average island size as a function of *K*, for a constant surface coverage. The two dependencies seen in the figure correspond to varying the number of deposition steps (triangles) and diffusion steps (squares). Both dependencies are decreasing power-law functions of *K*. However, it is evident from the graph that the effect of deposition rate's change is more pronounced than the effect of diffusion change. The corresponding power laws are -0.54 and -0.31, respectively. This difference arises because of different duration of deposition in these two cases. Indeed, our results obtained by varying the number of diffusion steps (at constant coverage) correspond to the same deposition time of 1 min. In contrast, varying the number of deposition steps at a constant coverage results in a decrease of the duration of deposition in proportion to $1/K$. As demonstrated in Fig. 7(c), duration of deposition is an important factor limiting the island size, which results in the faster decrease of the size when the duration of deposition decreases. The point of intersection of the two dependencies in Fig. 9 corresponds to similar durations of deposition.

The overall power-law dependencies $\sim 1/K^{\gamma}$ that we have obtained are in agreement with the analytical scaling law [8, 24]. However, depending on whether the diffusion or deposition steps were varied at a *constant coverage*, the corresponding powers differ by more than 40%. This is another example demonstrating that caution is required when applying the basic scaling laws to analyze the PVD processes, whose versatility should be accounted for carefully.
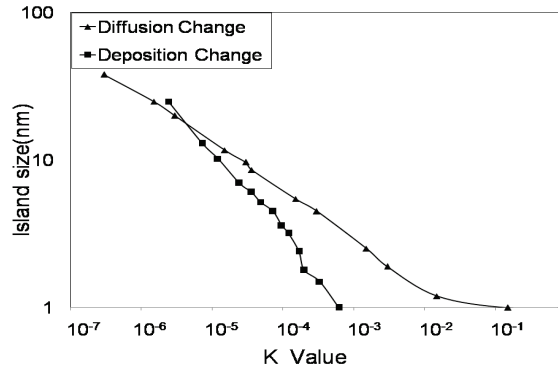
Figure 9: Average size of islands as a function of the kinetic parameter K, obtained by varying the number of diffusion steps at a constant 50% coverage (triangles), and by varying the number of deposition steps at a constant 23% coverage (squares), for 300 K deposition of Ag with Model 1.

3.4 Effect of diffusivity and temperature

From PVD practice it is known that the islands' size and density are extremely sensitive to temperature [10–12]. According to Eqs. (2.2)-(2.4), in our model temperature determines the surface diffusivity through two terms, the number of diffusion steps N_{diff} representing the surface mobility of unbounded adatoms (Eqs. (2.2)-(2.3)), and the probability P describing the interaction of adatoms with stable islands (Eq. (2.4)).

Firstly, we have varied the number of diffusion steps alone, without considering the corresponding change of the probability P. Fig. 10 demonstrates how the change in the number of diffusion steps in our simulation affects the island size with fixed percentage of coverage. This function is reasonably represented by an increasing scaling-low dependence $\sim 1/N_{diff}^{\gamma}$ with the power of 0.3, which is, in fact, the inverse of the corresponding curve in Fig. 9. It should be also noted that the maximum addressable value of N_{diff} is limited by the conditions at which one large cluster is formed, which depends on size of the system and the coverage considered.

Next, we have investigated the complete impact of temperature on the surface morphology by varying T in both Eqs. (2.3) and (2.4). Figs. 11(a,b) show the effect of temperature for two examples of metals and two different model substrates. Below 200 K, diffusion is very slow and islands hardly form over the time of the simulation. This explains the initial portions of the dependencies in Figs. 11(a) and (b), as well as the corresponding morphologies on Fig. 12, where only minor islands are detected, if any. It should be noted that a similar trend was reported in experiments for Ag deposition in [10]. More dramatic growth is observed in the temperature range 300-400 K, where coarsening by the Ostwald ripening becomes increasingly important when the temperature increases. Beyond 400 K, however, the increase of island size with temperature slows down slightly.

Figs. 11(a,b) demonstrates the effect of different activation and lateral bonding energies that correspond to two different metals and two different models, and Fig. 12 shows
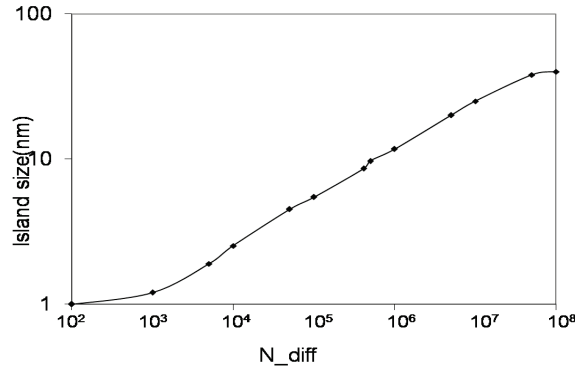
Figure 10: Average size of islands as a function of the number of diffusion steps N_{diff} (see Eq. 2.2) at a constant surface coverage ($\theta = 0.5$) for Ag deposition with Model 1.

(a)   (b)
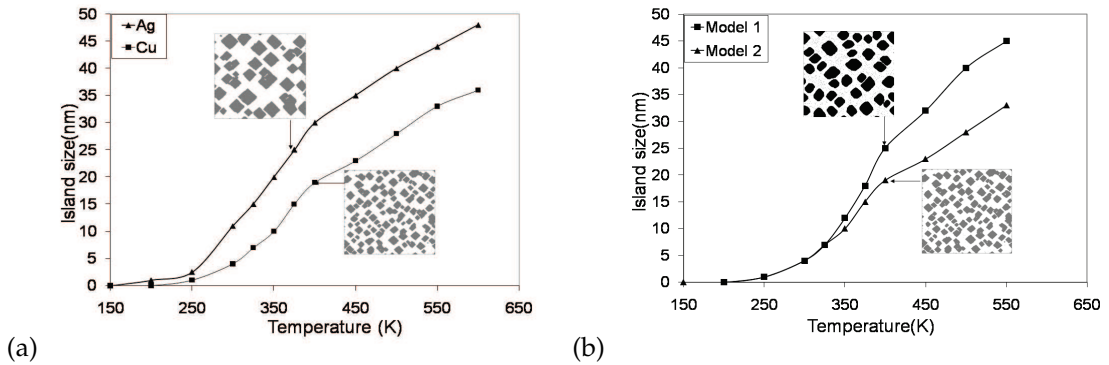
Figure 11: Average size of islands as a function of temperature at a constant coverage ($\theta = 0.5$) for (a) two metals Cu and Ag with Model 2 (a), and Cu with Model 1 and Model 2. The size of the modeled area shown in the insets is 100nm×100nm

the corresponding snapshots at various temperatures for Ag and Cu. Since Cu has higher activation energy for surface diffusion, the corresponding number of diffusion steps is lower than for Ag. As a result, we observe that island size is smaller in the case of Cu than for Ag deposition at similar temperatures.

Finally, Fig. 13 presents the density of islands as a function of temperature for Cu and Ag using Model 1. Clearly, lesser density of islands is observed at higher temperature with fixed surface coverage. However, the dependencies in Fig. 13 cannot be described by a simple dependence (1.1) with a single activation energy U. The numeric dependencies rather show a crossover from a two Arrhenius-like regimes with different activation energies, which occurs at temperatures close to 300°K. This behavior is typically observed in experiments [8, 10–12], and explained by the increasing impact of Ostwald ripening (also associated with reversible jumping) at increased temperatures.

(a)

(b)
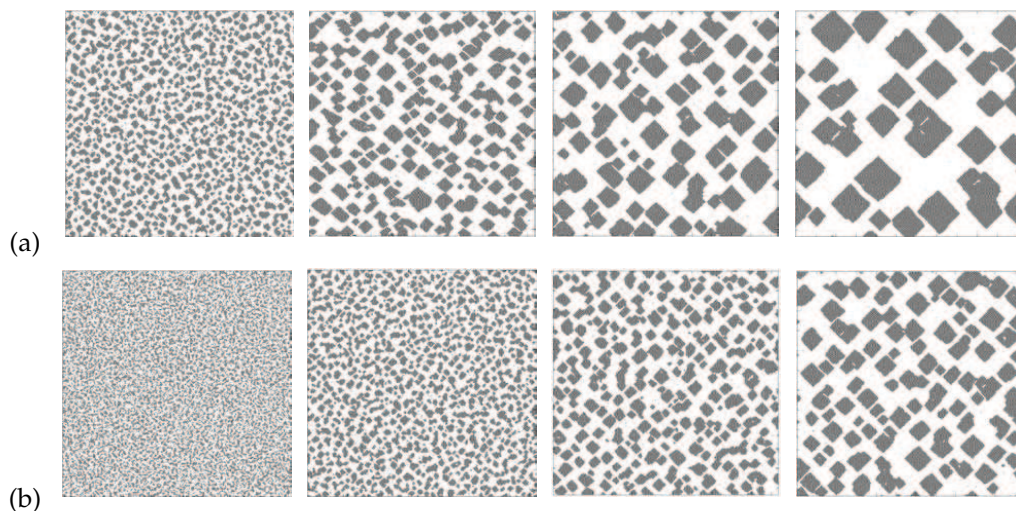
Figure 12: Simulated surface morphologies (Model 2) at temperatures of 250K, 300K, 350K and 400K for 1 min deposition at $R = 0.0093$ML/sec for (a) Ag and (b) Cu. The surface coverage is $\theta = 0.5$. The size of the modeled area is 100nm $\times$ 100nm.
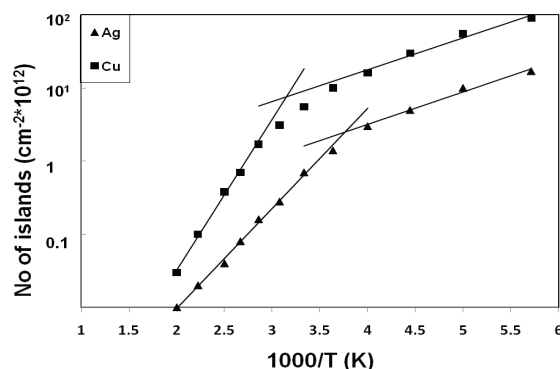
Figure 13: Average density of islands as a function of temperature for Cu and Ag with Model 1. The surface coverage is $\theta = 0.5$.

4 Summary

In this paper we present a KMC simulation for plane-view 2D morphologies of metallic nanoclusters during physical vapor deposition. Two models for the symmetry of the lateral interactions between adatoms have been investigated. One of these corresponds (100) crystalline islands with FCC symmetry, and the other one adopts the primitive lattice, which leads to softer shapes of deposited islands, and may better represent formation of nanoscale islands on non-crystalline substrates such as glass.

We have studied the impact of the variable process conditions such as the deposi-

tion rate, duration, and temperature, on the 2D morphologies of growing nanocrystals for two different model materials. We have demonstrated that the impact of deposition rate on the surface morphology depends dramatically on the other process conditions, e.g. whether the duration of deposition or the amount of deposited material is kept constant. Our analysis clarifies the origin of this difference, as well as provides an insight into the capabilities to control the surface morphology by varying the deposition rate and temperature for various deposition processes.

Analysis of the numeric results in the light of the corresponding analytical scaling laws shows a reasonable agreement in a few cases when the scaling laws are applicable. These include the dependence of the average island density deposition rate with a constant surface coverage, and the dependence of the average density of islands on the number of diffusion jumps with unchanged conditions of adatom attachment-detachment. However, many regimes relevant to practical PVD conditions require a higher flexibility. The classic scaling laws, although very useful for understanding the basic physical trends, are not always flexible enough to capture efficiently all the regimes of deposition. This emphasizes the importance of efficient direct simulations of the deposition process. Furthermore, KMC simulations also provide important information on the detailed surface morphology, which is a mandatory component required for a detailed understanding of the outcomes of deposition of nanocrystals.

As discussed throughout the paper, our simulated dependencies of the surface morphologies match benchmark experimental observations from the literature. This includes the overall shape of the islands observed, the dependencies of the morphological trends on the deposition rate, and the realistic temperature of cross-over in the temperature dependence obtained numerically. These examples demonstrate that our model is a viable approach that adequately represents major trends of 2D surface morphologies during deposition. Our expectation is that numerical models like this can be employed to efficiently predict the outcomes of nanocrystal deposition, and rationally direct selection of optimal process conditions for nanofabrication. We are currently extending of our modeling for 3D multilayer morphologies and a study of these as a function of conventional instrument parameters, such as pressure or voltage, to facilitate practical applications for PVD process optimization.

Acknowledgments

References

[1] K. Reichelt, Nucleation and growth of thin films, Vacuum, 38 (1988) 1083.
[2] J.G. Amar and F. Family, Kinetics of submonolayer and multilayer epitaxial growth, Thin Solid Films 272 (1996) 208.

[3] J.M. Pomeroy and J.D. Brock, Critical nucleus phase diagram for the Cu (100) surface, Phys. Rev. B 73, (2006) 245405.

[4] J.A. Venables,G.D.T. Spiller and M. Hanbucken, Nucleation and growth of thin films, Rep.Prog. Phys, 47, (1984) 399.

[5] J.A. Venables, Nucleation and growth processes in thin film formation, J. Vac. Sci. Technol. B, 4 (1986) 870.

[6] J.A. Venables, Atomic processes in crystal growth, Surf. Sci. 299(1994) 798.

[7] C. Ratsch and J.A. Venables, Nucleation theory and the early stages of thin film growth, J. Vac. Sci. Technol. A. 21, (2003) S96.

[8] H. Brune, G.S. Bales, J. Jacobsen, C. Boragno, and K. Kern, Measuring surface diffusion from nucleation island densities, Phys. Rev. B 60 (1999) 5991.

[9] H. Shirakawa and H. Komiyama, Migration-coalescence of Nanoparticles During Deposition of Au, Ag, Cu, and GaAs on Amorphous SiO2, J. of Nanoparticle Research 1 (1999) 17.

[10] S. Frank, H. Wedler, R.J. Behm, J. Rottler, P. Maass, Approaching the low-temperature limit in nucleation and two-dimensional growth of fcc (100) metal films Ag/Ag(100), Phys. Rev. B 66 (2002) 155435.

[11] C.M. Zhang, M.C. Bartelt, J.M. Wen, C.J. Jenks, J.W. Evans and P.A. Thiel, Submonolayer island formation and the onset of multilayer growth during Ag/Ag(100) homoepitaxy, Surf. Sci. 406 (1998) 178.

[12] J.A. Stroscio, D.T.Pierce, and R.A. Dragoset, Homoepitaxial growth of iron and real space view of Refection-High-Energy-Electron diffraction, Phys Rev. Lett. 70-23 (1993) 3615.

[13] P. Bruschi, P. Cagnoni, and A. Nannini, Temperature-dependent Monte Carlo simulations of thin metal film growth and percolation, Phys. Rev. B 55, (1997) 7955.

[14] P. Heino, H. Hakkinen, and K.Kaski, Molecular-dynamics study of copper with defects under strain, Phys. Rev. B 58-2, (1998) 641.

[15] D.Wolf, V. Yamakov, S.R. Phillpot, A. Mukherjee, and H. Gleiter, Deformation of Nanocrystalline Materials by Molecular-Dynamics Simulation: Relationship to Experiments, Acta Materialia 53 (2005) 1.

[16] S. Erkoc, Stability of Gold Clusters: Molecular-Dynamics Simulations, Physica E, 8 (2000) 210.

[17] H. Huang, G.H. Gilmer and T.D. de La Rubia, An atomistic simulator for thin film deposition in three dimensions, J. Appl. Phys. 84 (1998) 3636.

[18] S. Frank, and P. A. Rikvold, Kinetic Monte Carlo simulations of electrodeposition: Crossover from continuous to instantaneous homogeneous nucleation within Avrami's law, Surf. Sci. 600 (2006) 2470.

[19] L.G. Wang and P. Clancy, Kinetic Monte Carlo simulation of the growth of polycrystalline Cu film, Surf. Sci. 473 (2001), 25.

[20] F.F Abraham and G.M. White, Simulation Time Versus Real Time in Computer Simulation of Vapor Deposition, J. Appl. Phys. 41 (1970) 184.

[21] H.L. Wei, Z.L. Liu and K.L. Yao, Influence of microstructure of substrate surface on early stage of thin film growth, Vacuum 56 (2000), 185.

[22] L. Nurminen, A. Kuronen and K. Kaski, Kinetic Monte Carlo simulation of nucleation on patterned substrates, Phys. Rev. B 63 1-7 (2000), 035407.

[23] D.P. Landau, S. Pal and Y. Shim, Monte Carlo Simulations of Film Growth, Comput. Phys. Comm. 121 (1999) 341.

[24] O. Biham, I. Furman, M. Karimi, R. Kennett, G. Vidali and H. Zeng, Models for diffusion

and island growth in metal monolayers, Surf. Sci. 400 (1998), 29.

[25] M. Hildebrand and A. S. Mikhailov, Mesoscopic modeling in the theory of reactive adsorbates, J. Phys. Chem. 100 (1996) 19089.

[26] L.J. Friedrich, S.K. Dew, M. Brett, and T. Smy, Thin film microstructure modelling through line-segment simulation, Thin Solid Films 266 (1995) 83.

[27] J.W. Evans, P.A. Thiel and M.C. Bartelt, Morphological Evolution during Epitaxial Thin Film Growth: Formation of 2D Islands and 3D Mounds," Surface Science Reports, Surface Science Reports 61 (2006) 1.

[28] In this work, the interatomic distances for Cu and Ag were taken similar in order to facilitate comparison of the kinetic factors. The slight (10

[29] K. Kambe, Cohesive Energy of Noble Metals, Physical Review, 99 (1955) 419.

[30] In Model 1, an atom has 8 lateral neighbors and 9 neighbors below on the substrate, so the total number of neighbor atoms is 17. Model 2 adopts 4 lateral neighbors and 5 effective bonds with the substrate. Thus, our estimate of lateral bonding based on the measured cohesive energy for Cu provides the energy per bond of approximately 0.20 eV for Model 1, and 0.39 eV for Model 2. For Ag the values are 0.17 and 0.32 eV, respectively.

[31] J. Uppenbrink and D. J. Wales, Structure and energetics of model metal clusters, J. Chem Phys, 96 (1992) 8520.

[32] W. Eckstein, Computer simulation of ion-solid interactions, Springer-Verlag, Berlin, 1991

[33] The description of the SRIM code can be found at `http://www.srim.org/`.